

Structural Remodeling Mechanism of the Toxic Amyloid Fibrillary Mediated by Epigallocatechin-3-gallate

Nan Zhang,* Chaoren Yan, Changji Yin, Xiaoling Hu, Ping Guan, and Yuan Cheng*

Cite This: *ACS Omega* 2022, 7, 48047–48058

Read Online

ACCESS |



Metrics & More

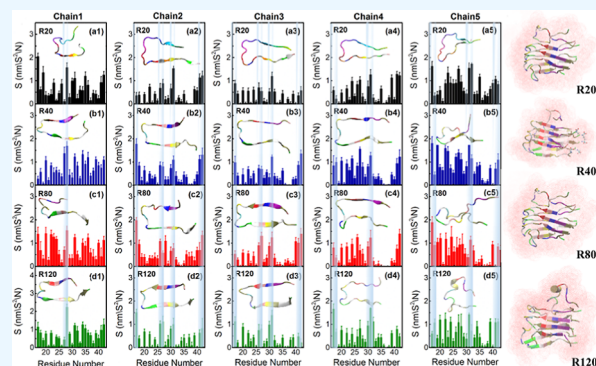


Article Recommendations



Supporting Information

ABSTRACT: Numerous therapeutic agents and strategies were designed targeting the therapies of Alzheimer's disease, but many have been suspended due to their severe clinical side effects (such as encephalopathy) on patients. The attractiveness for small molecules with good biocompatibility is therefore restarted. Epigallocatechin-3-gallate (EGCG), extracted from green tea, is expected to be a promising small-molecule drug candidate, which can remodel the structure of preformed β -sheet-rich oligomers/fibrils and then effectively interfere with neurodegenerative processes. However, as the structure of non-fibrillary aggregates cannot be directly characterized, the atomic details of the underlying inhibitory and destructive mechanisms still remain elusive to date. Here, all-atom molecular dynamics simulations and experiments were carried out to elucidate the EGCG-induced remodeling mechanism of amyloid β ($A\beta$) fibrils. We showed that EGCG was indeed an effective $A\beta$ fibril inhibitor. EGCG was capable of mediating conformational rearrangement of $A\beta_{1-42}$ fibrils (from a β -sheet to a random coil structure) and triggering the disintegration of fibrils in a dose-dependent manner. EGCG redirected the structure of $A\beta$ by breaking the β -sheet structure and hydrogen bonds between peptide chains within the $A\beta$ protofibrils, especially the parallel β -strand (L₁₇VFFAEDVGS₂₆). Moreover, reduced solvent exposure and multisite binding patterns all tended to induce the conformation conversion of $A\beta_{17-42}$ pentameric protofibrils, destroying pre-formed fibrils and inhibiting continued fibril growth. Detailed data analysis revealed that structural features of EGCG with abundant benzene ring and phenolic hydroxyl moieties preferentially interact with the parallel β -strands to effectually hinder the interaction of the interpeptide chain and the growth of the ordered β -sheet structure. Furthermore, experimental studies confirmed that EGCG was able to disaggregate the preformed fibrils and alter the protein structure. This study will enable a deeper understanding of fundamental principles for design of structural-based inhibitors.



INTRODUCTION

With the growth of the aging population, the huge cost of treating Alzheimer's disease (AD) has been a serious challenge. In the United States, the number of Americans with AD who are over 65 is expected to increase from 55 billion in 2019 to 88 million in 2050.¹ The total annual cost of people's wellness care, long-term care, and hospice care is estimated to increase from \$256.7 billion in 2020 to more than \$ 1.1 trillion in 2050.^{2,3} Tremendous efforts on potential therapies have been ongoing without producing a drug or novel therapeutics which is capable of curing AD. Since AD is accompanied by plentifully disparate pathology mechanisms, various approaches have been used to search for treatments, such as anti-inflammatory and antihypertensive drugs, passive and active immunity, neuroprotective agents, β - and γ -secretase enzyme inhibitors, tau aggregation inhibitors, and metal chelators.^{4–7} In addition to soluble amyloid polypeptide (APP), γ -secretase also cleaves a plethora of other proteins with important biological functions, leading to worsening of the recipient's condition. Thus, the inhibition of the enzyme's function is no longer considered to be a good approach.^{8–10}

Instead, the breakthrough achieved with $A\beta$ -specific antibodies for passive immunization is considered to be the most promising. However, phase III clinical trials were also suspended due to several severe encephalopathy cases. Beneficial results are only produced in ApoE4 carriers and still have side-effects in numerous patients.^{11,12} Recent announcement of Biogen claims that they will resurrect an Alzheimer's drug declared a failure in March 2019,¹³ an antibody named aducanumab designed to aim at the beta-amyloid protein in the brain. Thus, the appeal for small molecules with good biocompatibility was reinitialized.

Various small molecules with anti-aggregation potential (also deemed anti-aggregates) have been screened for $A\beta$ fibrils or

Received: September 16, 2022

Accepted: December 1, 2022

Published: December 13, 2022



fibril precursors. Among them, the peptide and its derivative, usually a modified LFFFA sequence taken from an assumed nucleation site, are anticipated to self-complementarily bind to the central hydrophobic cluster of $A\beta$.^{14,15} For example, Soto et al. proposed LPFFD, a β -sheet breaker, which reserved the high affinity with the LFFFA region ($A\beta_{17-21}$) but disordered its β -sheet domain.¹⁶ Other examples recently studied involves inositol,¹⁷ curcumin,¹⁸ and (-)-epigallocatechin-3-gallate (EGCG) (Figure 1a).¹⁹ Among them, polyphenols with

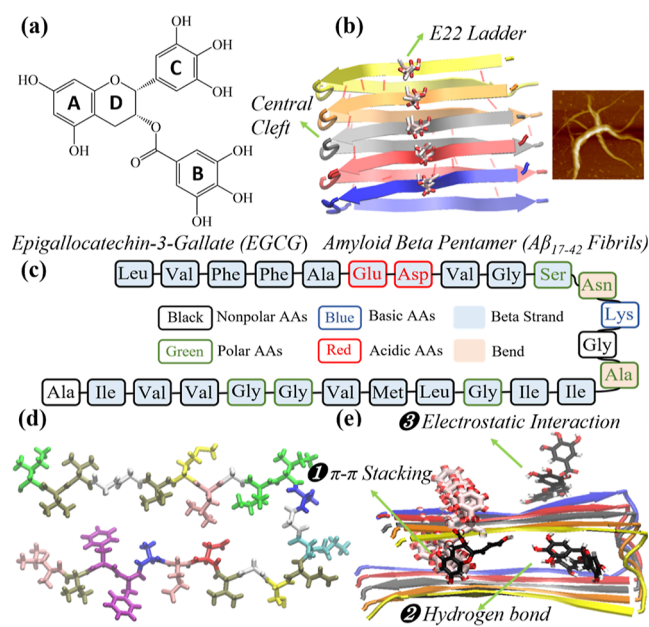


Figure 1. Structural properties of EGCG and amyloid fibrils. (a) Four benzene rings from EGCG defined as A, B, C, and D figuring out four rational regions for the hydrophobic interaction with amyloid fibrils. (b) Top view of the U-shaped $A\beta$ fibril exhibiting the position of the individual peptide chains (color-coded according to their stacked sequences). The AFM images on the left represent the fiber morphology formed. (c) The color of the amino acid (AA) type (including the nonpolar, polar, basic, and acidic AA residues) is encoded in black, green, blue, and red. The types of secondary structures within the chain are identified by light blue and light pink. The insert images are the detailed view of the intramolecular hydrogen bonding interactions in one peptide chain of the $A\beta_{17-42}$ pentamer with residues $L_{17}-A_{42}$. (d) Schematic diagram of the anti-aggregation and disassembly effects of EGCG on $A\beta$ formation.

antioxidant activity and antiviral and anti-inflammatory properties extracted from green tea, namely, EGCG, were small molecules with the greatest therapeutic potential to intervene in the on-pathway process of amyloid formation and perturb off-pathway oligomers.^{20,21} The increasing evidence indicates the capability of EGCG to bind and divert amyloidogenic peptides into non-toxic aggregates during the self-association stage, which has evoked intensive studies on the EGCG and amyloidogenic peptide complexes.²²⁻²⁴ EGCG has been reported to foster the release of soluble APP in the human neuroblastoma and mouse hippocampus.²⁵ Previous studies have also shown that EGCG has a neuroprotective effect on ischemia-induced brain impairment caused by restraining neuronal cell death due to inflammatory and oxidative stress.²⁶ Besides, the preformed mature amyloid fibrils/oligomers exhibited a reduction in cytotoxicity when bound with EGCG and were effectively redirected into smaller

amorphous non-pathway aggregates with less toxicity.²⁷ Surprisingly, a solid theoretical foundation of the inhibitors– $A\beta$ protein interaction mechanism is far from complete, and generalized guidance based on structural characterization validated by experiments is in urgent demand.

Understanding of the topology and structural properties of molecules is critical for design of inhibitors. Regarding the $A\beta_{17-42}$ oligomer we studied, its U-shaped topology (Figure 1b,c) is formed by the two β -strands in each monomeric peptide connected by a turn.²⁸ The monomeric peptides grow and stack in the longitudinal direction, thus shaping into parallel and anti-parallel β -sheets. Previous studies have provided preliminary hints/information on structural characteristics of $A\beta$ -binding ligands: for example, a polar region formed by D23–K28, an E22 ladder formed by E22 side chains of a cross- β -sheet, and the central cleft formed in the U-shaped turn.²⁹ Besides, EGCG has not only abundant hydroxyl groups that can interact with hydrogen-bonded donors and acceptors but also benzene rings that are in favor of interacting with the hydrophobic moieties of β -sheet fragments.³⁰ In many experiments, it has been proved that EGCG selectively binds to the backbone of misfolded peptides with a prominent β -sheet structure. EGCG disturbs the N-terminal residues of $A\beta$, and the chemical shift changes induced by EGCG occur mainly in the central hydrophobic region of $A\beta$.³¹ Other studies have further confirmed that changes in $A\beta_{40}$ oligomer residues were responsible for the cytotoxicity reduction.³² However, to date, the molecular basis for EGCG-induced remodeling from toxic $A\beta$ fibrils/oligomers to non-toxic oligomers remains elusive. The relative binding affinity of EGCG toward monomeric peptides and oligomers and the interference of EGCG with fibril assembly are still unclear. Thus, it is crucial to elucidate the molecular mechanism of EGCG as an amyloid inhibitor decomposing the preformed protofibrils.

In our work, we discussed the dose dependence of EGCG-mediated structural redirection and the structural redirection mechanism between EGCG and preformed $A\beta_{17-42}$ pentameric fibrils using all-atom molecular dynamics (MD) simulations.^{33,34} Detailed atomistic-scale analysis revealed that the disaggregation of $A\beta_{17-42}$ oligomers was driven by electrostatic and van der Waals (VdW) interaction. The EGCG influenced the structural behavior and hydrogen bonding states; thus, the distribution of binding sites of EGCG–amyloid and the effect on the structure of the $A\beta_{17-42}$ oligomer can significantly screen out the preferential target regions with EGCG. Experimental studies including atomic force microscopy (AFM), thioflavin-T (ThT) fluorescence assay, and circular dichroism (CD) confirmed that EGCG was capable of disaggregating the preformed fibrils. Moreover, we have discovered a “solvent shielding effect” on amyloid introduced by EGCG by analyzing surface area of each amino acid (AA) residue exposed to the solvent. Our results showed that EGCG redirected amyloid fibrils into disordered aggregates through hydrophobic interactions and introduced solvent-mediated effects for inhibiting fibril formation. These findings indicated that $A\beta$ inhibitors can be further developed to prevent and break down amyloid fibrils by utilizing the good biocompatibility and anti-inflammatory and anti-aggregation effects of EGCG. By combining the simulation results with the experimental evidence, the correlation between the structural features of EGCG and binding behaviors to $A\beta_{17-42}$ oligomers was further explored, thus providing valuable information for design of structural-based oligomer inhibitors.

MATERIALS AND METHODS

Materials and Reagents. $A\beta$ protein, EGCG, and hexafluoroisopropanol (HFIP) were purchased from Aladdin Biochemical Technology Co., Ltd. (Shanghai, China); ThT was ordered from Macklin Biochemical Technology Co., Ltd. (Shanghai, China); Dulbecco's phosphate buffered saline (PBS) buffer solution was purchased from Gibco BRL (Carlsbad, CA, USA); ethanol comes from Tianjin Kemeiou Chemical Reagent Company. All other chemicals were commercially available and used without further purification.

Physicochemical Characterization. AFM (Bruker Dimension FastScan and Dimension Icon) was performed to investigate the morphologies of $A\beta$ protein before and after aggregation. The fluorescence spectrum of $A\beta$ protein before and after aggregation was tested using a fluorescence spectrophotometer (F-320, China); the secondary structure of $A\beta$ protein before and after aggregation was measured using a Chirascan CD spectrometer (CD, Applied Photophysics, UK).

Simulation Methods for the Interaction between $A\beta$ and EGCG. *Structural Optimization and Parameterization of EGCG.* The geometric structure of EGCG was built from the GaussView05 program.³⁵ The configuration optimization of EGCG was performed by the Hartree–Fock method on the B3LYP/6-31G*(d) basis by employing the Gaussian16 program.^{36,37} Then, the electrostatic potential (ESP) can be obtained at the same parameters correspondingly. To acquire the topology files, the Antechamber program in the AmberTools package was used to fit the restrained ESP charge, and then, the generalized Amber force field was adopted to parameterize for bonded interaction of the EGCG molecule for subsequent MD simulations.³⁸ As shown in Figure 1a, the four rings in the EGCG molecule were labeled A, B, C, and D, where A, B, and C were aromatic rings.

Design and Construction of the EGCG– $A\beta$ System Model. The initial structure of the fibrillar $A\beta_{17-42}$ pentamer was obtained from the Protein Data Bank (PDB code: 2BEG).³⁹ The selected pentamer with a rich β -sheet structure was the predominantly hydrophobic core fragment of $A\beta_{17-42}$, which can represent typical hydrophobic fibrils while significantly reducing the modeling cost of $A\beta_{17-42}$ fibers with a longer and more complex structure. To elaborate the effect of the EGCG concentration on the inhibitory and remodeling mechanism, four systematic models of the EGCG + $A\beta_{17-42}$ pentamer were set up for the study with various molar ratios of EGCG to $A\beta_{1-42}$ fibril, which were 1:20, 1:40, 1:80, and 1:120 (deemed R20, R40, R80, and R120, $A\beta_{1-42}$ fibril to EGCG on a molar basis). As shown in Figure 2, for the initial coordinate of each system, the $A\beta_{17-42}$ pentamer was immersed in the center of a suitable simulation box filled with TIP3P water, and EGCG was randomly distributed around the $A\beta_{17-42}$ pentamer, of which the minimal distance from the solute to the box wall was 1.2 nm. The simulation box sizes were $7.58 \times 7.58 \times 7.58$, $12.51 \times 12.51 \times 12.51$, $17.96 \times 17.96 \times 17.96$, and $21.96 \times 21.96 \times 21.96$ nm³, with a total of 52,968, 196,113, 430,381, and 580,551 atoms in the respective systems, respectively.

MD Simulation Method of EGCG– $A\beta$ Interaction. We performed all MD simulations using GROMACS 5.1.2 and adopted the AMBER03 force field to parameterize the fibrillar $A\beta_{17-42}$ pentamer.^{40,41} The solvent used was the TIP3P water model, and each system was neutralized by five counterions (Na⁺).⁴² The temperature at 310 K was controlled by the V-

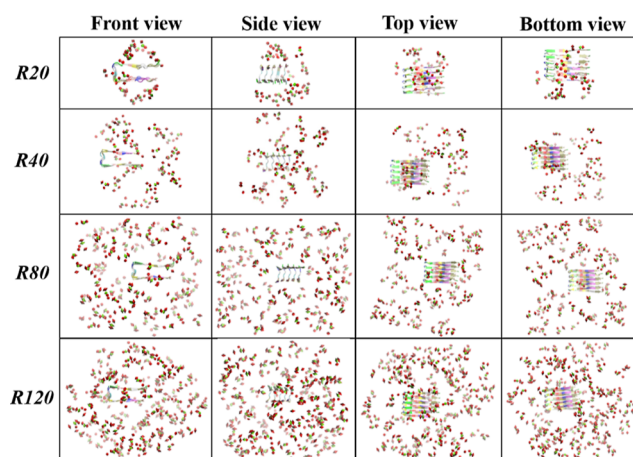


Figure 2. Initial configurations of the $A\beta_{17-42}$ pentamer with EGCG. R20, R40, R80, and R120 represent different cases with concentrations of EGCG as 1:20, 1:40, 1:80, and 1:120, respectively. Initially, EGCG was randomly distributed inside the water box. Water molecules are not shown for clarity.

rescale temperature coupling.⁴³ The barostat with a constant pressure of 1 atm was described by the Berendsen pressure coupling method.⁴⁴ The LINCS algorithm was utilized to restrain the atomic bonds of the organic molecules and $A\beta_{17-42}$ pentamer.⁴⁵ The cut-off distance for non-bonded interactions was set at 1 nm. The electrostatic interactions were treated with the particle mesh Ewald method with a cut-off of 1 nm.⁴⁶ Periodic boundary conditions were implemented in all three directions. Energy minimization was carried out using the steepest descent algorithm prior to performing dynamic simulations. MD simulations for the systems were carried out for 1000 ns with a time step of 0.002 ps per integration step.

All molecular structures were visualized using the VMD program.⁴⁷ The secondary structure data was calculated by the built-in Timeline program using the STRIDE algorithm and dictionary secondary structure of protein method.^{48,49} The contact number of atoms was defined as the number of heavy atom pairs whose interatomic distance between EGCG and the model $A\beta_{17-42}$ pentamer was less than 6.0 Å. The interaction energies were determined by calculating the sum of the vdW and electrostatic energies between the $A\beta_{17-42}$ pentamer and the EGCG.

Experimental Procedure of Aggregation and Disaggregation of $A\beta$. *Preparation and Formation of $A\beta$ Fibrils.* The fresh lyophilized $A\beta_{1-42}$ powder was dissolved in HFIP and stored for 2 h. Then, the sample was sonicated in an ice bath for 30 min to remove possible $A\beta$ oligomers. Before the CD test, the samples were quickly dried under nitrogen. The obtained samples were dissolved in PBS solution to ensure that the concentration of the $A\beta_{1-42}$ monomer is 0.5 mg mL⁻¹ and immediately transferred to the CD test. The samples were then incubated in a shaker at 37 °C for a certain period of time and immediately tested for CD. Each sample was tested three times, and the average was taken. For more accurate test results, we shook the cuvette to obtain a better dispersion before testing. The parameters of the circular chromatograph were set as follows: the bandwidth is 2.0, the wavelength scanning range is 190–280 nm, the frequency interval is 1 nm, and the width of the quartz cuvette is 1 mm. The prepared $A\beta_{1-42}$ monomer was dissolved in PBS (0.2 M, pH = 7.4), and

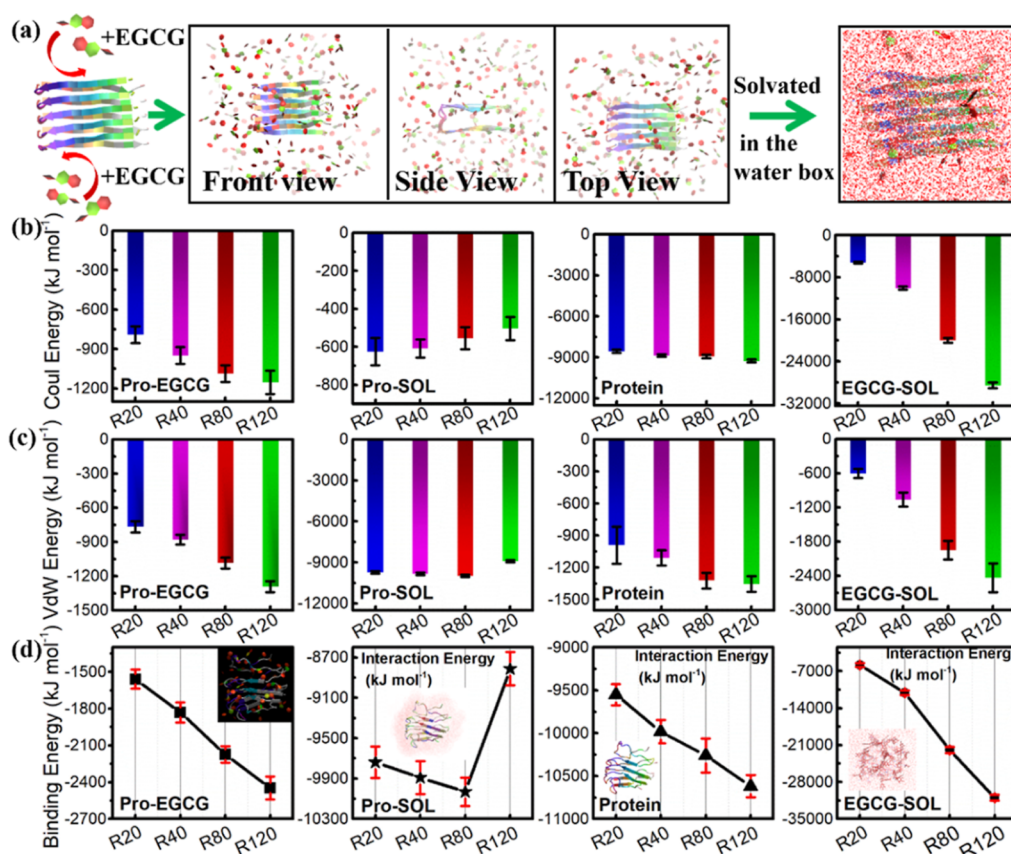


Figure 3. (a) Taking the case of R120 as an example, the initial setup of the system is shown. Comparison of Coulombic (Coul) (b), VdW (c), and binding energies (d) of the $A\beta_{17-42}$ oligomer (Pro) and EGCG in four cases. Each system averaged from three independent trajectories. The numbers “1”, “2”, “3”, and “4” after the letter represent the $A\beta_{17-42}$ oligomer–EGCG, EGCG–solvent (SOL), $A\beta_{17-42}$ oligomer itself, and EGCG–SOL, respectively. The insert images are the equilibrium configuration of the $A\beta_{17-42}$ oligomer induced by EGCG (e.g., the case of R20).

the concentration of the $A\beta_{1-42}$ monomer was still 0.5 mg mL^{-1} . Subsequently, we used AFM to test the morphology changes of $A\beta$ fibrils at different stages. The $A\beta_{1-42}$ monomer was cultured in a shaker at 37°C , and a $20 \mu\text{L}$ sample was taken from the cultured sample at a certain time. Before the test, the sample was diluted with alcohol and dropped on a silicon wafer to air dry.

Tracking Process of Inhibition and Clearing $A\beta$ Fibrils with EGCG. The prepared $A\beta_{1-42}$ monomer was dissolved in PBS (0.2 M , $\text{pH} = 7.4$) to ensure that the concentration of the $A\beta_{1-42}$ monomer was 0.5 mg mL^{-1} . The sample was shaken slowly in a shaker at 37°C , and CD was continuously tested during the shaking process until the $A\beta_{1-42}$ monomer formed CD of amyloid fibrils. Subsequently, EGCG (98%) was added to the cultured $A\beta_{1-42}$ amyloid fiber stock solution in a molar ratio of 1:20, 1:40, 1:80, and 1:120 and continued to be shaken at 37°C , and CD was used to continuously detect the extent of $A\beta_{42}$ amyloid fiber dissolution at four EGCG concentrations. Each sample was scanned three times and averaged. The parameters of the circular chromatograph were the same as the abovementioned. Additionally, we used the same series of ratios between EGCG and the cultured $A\beta_{42}$ amyloid fibril stock solution (37°C , 24 h). Finally, the sample was diluted with alcohol before the test and dropped on mica flakes to air dry and then subjected to the AFM measurement. For the ThT (Mulgrave, Australia) test, the prepared $A\beta_{1-42}$ monomer was dissolved in PBS (0.2 M , $\text{pH} = 7.4$), and ThT was added into the above-mentioned solution to ensure that the concentration

of the $A\beta_{1-42}$ monomer and ThT, respectively, was 0.5 mg mL^{-1} and $6.4 \mu\text{g mL}^{-1}$. The sample was shaken slowly in a shaker at 37°C until amyloid fibers were formed. This process used a fluorescence spectrophotometer to continuously detect the fluorescence intensity of the sample, which was the detection of the aggregation process. After the formation of the $A\beta_{1-42}$ amyloid fibril, EGCG was added to the cultured $A\beta_{42}$ fibril stock solution with the same series of ratios and was continued to be shaken slowly at 37°C for about 24 h. This process also used a fluorescence spectrophotometer to continuously detect the fluorescence intensity of the sample, namely, the detection of the depolymerization process of the $A\beta_{1-42}$ fibril. The excitation wavelength of the fluorescence spectrophotometer was set to 440 nm , and the fluorescence intensity at an emission wavelength of about 485 nm was recorded. This process always kept the setting parameters unchanged.

RESULTS AND DISCUSSION

Structural Remodeling and Disaggregation Mechanism of $A\beta_{17-42}$ Oligomers Induced by EGCG. We conducted MD to study the EGCG-induced $A\beta_{17-42}$ pentameric fibril ($A\beta_{17-42}$) structural remodeling at the molecular level (Figure 1d). For the setup of the system, see Figure 3a. First, the root mean square deviation (rmsd) (Figure S2a), the radius of gyration (R_g) (Figure S2b), and the contact number of heavy atoms (no. of contact) (Figure S2c) between $A\beta_{17-42}$ and EGCG were obtained to determine the

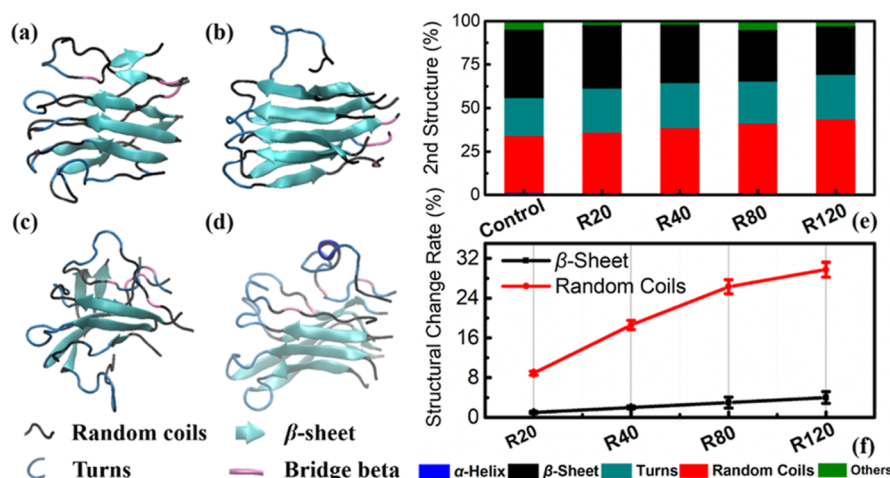


Figure 4. Representative snapshots of the $A\beta_{17-42}$ oligomer's conformation with EGCG in the cases of (a) R20, (b) R40, (c) R80, and (d) R120. (e) Secondary structure contents of $A\beta_{17-42}$ in the absence and presence of EGCG molecules. The average content value of each secondary structure (random coil, β -sheet, salt bridge, and turn) is calculated based on the last 200 ns data. Varying colors represent diverse types of secondary structures. (f) Loss rate of the main secondary structure (β -sheet and random coils).

convergence of the MD simulation. The distribution range of the rmsd, R_g , and no. of contact in the last 200 ns oscillated around constant values, demonstrating that the overall structure of the four systems had equilibrated. To resolve the effect of the EGCG with various molar ratios on the conformational evolution of $A\beta_{17-42}$, we calculated the interaction energy of $A\beta_{17-42}$ -EGCG, $A\beta_{17-42}$ -SOL, $A\beta_{17-42}$, and EGCG-solvent (SOL) as shown in Figure 3. The binding energy (Figure 3d) is defined as the sum of Coulombic (Coul) (Figure 3b) and vdW (Figure 3c) interaction energy. As shown in Figure 3d1, the average binding energy between EGCG and $A\beta_{17-42}$ was -1558 ± 76 , -1830 ± 81 , -2174 ± 127 , and -2447 ± 94 kJ mol⁻¹, respectively, corresponding to R20, R40, R80, and R120 (the specific process is shown in Figures S3 and S4). Their interaction strength was positively correlated with the molar ratio of $A\beta_{17-42}$ /EGCG. EGCG destabilized $A\beta_{17-42}$ to counteract the interactions of $A\beta_{17-42}$ -SOL. However, the EGCG concentration had a slight impact on the interaction energy of $A\beta_{17-42}$ -SOL (Figure 3d2).

For the R120 system, surprisingly, the $A\beta_{17-42}$ -SOL interaction energy (-8811 ± 265 kJ mol⁻¹) was significantly lower than that of the other three cases, which may be because more abundant EGCG distributed around the fibril shielded the interaction between the protein and the SOL surrounding the protein. The change in interaction energy of $A\beta_{17-42}$ reduced inconspicuously (Figure 3d3). As shown in Figure 3d4, the interaction energy of EGCG-SOL including both Coul and VdW interaction items enhanced with the increase in the EGCG concentration (Figure 3b4,c4). The structural rearrangement of $A\beta_{17-42}$ pentameric fibrils reduced the energy of the entire system referring to intramolecular interactions of $A\beta_{17-42}$ and enhanced the intermolecular interactions of $A\beta_{17-42}$ -EGCG and $A\beta_{17-42}$ -SOL. Meanwhile, the electrostatic and VdW interactions of $A\beta_{17-42}$ -EGCG promoted this situation (Figure 3b,c). Note that the absolute value of the binding energy of $A\beta_{17-42}$ -SOL was much larger than that of the intramolecular interaction energy of $A\beta_{17-42}$, indicating that the SOL also played a crucial role in the dissociation of $A\beta_{17-42}$. As the interaction energy changed, the structure and conformation of $A\beta_{17-42}$ with the EGCG quickly became

unstable and experienced a structural transition (see the following discussion and Figure S5 for further information). It was obvious that EGCG-containing ample benzene rings and hydroxyl groups were in favor of forming p-p stacking, π - π stacking, and H-bond interaction, thus facilitating the interaction with the monomeric peptide chain in $A\beta_{17-42}$ and correspondingly weakening the intramolecular interaction within $A\beta_{17-42}$, which were consistent with the above-mentioned analysis of the binding energy.

Since the alteration of the protein's ordered state was closely related to its secondary structure, as shown in Figure 4, we analyzed the conformation conversion and the secondary structure contents of $A\beta_{17-42}$ with and without EGCG. The complete time evolution of the secondary structure of $A\beta_{17-42}$ during interaction with EGCG is shown in Figure S6. It can be visually seen from Figure 4a-d that EGCG initiated the disordering of the secondary structure of $A\beta_{17-42}$, leading to the first dissociation of the outmost peptide chain. We can also see from Figure 4e that the β -sheet content of $A\beta_{17-42}$ was $36.53 \pm 0.12\%$ in the case of R20, quite close to that ($39.24 \pm 2.1\%$) in the control system for $A\beta_{17-42}$ alone. As the EGCG molar ratio increased, the average β -sheet content value significantly reduced from $33.61 \pm 1.1\%$ (R40) and $29.65 \pm 0.4\%$ (R80) to $27.97 \pm 1.7\%$ (R120), while the composition of the random coil increased from $32.57 \pm 0.11\%$ (control) to $35.93 \pm 0.23\%$ (R20), $38.63 \pm 0.21\%$ (R40), $41.12 \pm 0.10\%$ (R80), and $43.56 \pm 0.20\%$ (R120). There were no obvious changes in the contents of the "turn" structure, indicating that they were insensitive to the changes in the EGCG's proportion. Furthermore, the structural loss rate of the β -sheet enhanced from 6.9% (R20), 14.3% (R40), and 24.4% (R80) to 28.7% (R120) (Figure 3f). Overall, the secondary structure change was dose-dependent. EGCG elicited a decline in the β -sheet structure of $A\beta_{17-42}$, and the loss of the β -sheet was observed to almost convert into a random coil completely. It demonstrated that the addition of EGCG to the $A\beta_{17-42}$ system could markedly restrain the continued formation of these β -sheet structures, thus suppressing $A\beta$ fibrillization.

The secondary structure of the protofibril is stabilized by hydrogen bonds (H-bonds) formed between monomeric peptide chains. H-bond interactions can not only change the

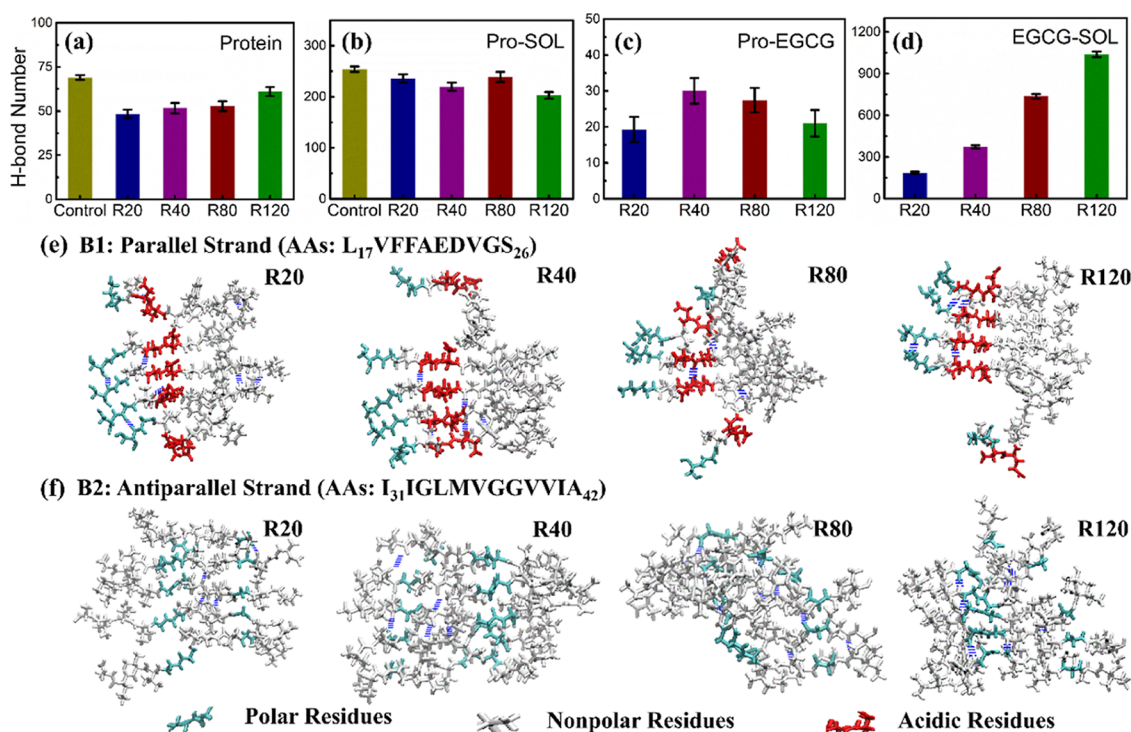


Figure 5. Hydrogen bond evolution to probe the disassembly mechanism of amyloid fibrils. Hydrogen bond number in $A\beta_{17-42}$ pentameric fibrils (a), $A\beta_{17-42}$ pentameric fibril–SOL (b), $A\beta_{17-42}$ pentameric fibril–EGCG (c), and EGCG–SOL (d). Respective representative snapshots of parallel strand (e) and antiparallel strand (f) refer to R20, R40, R80, and R120. Error bars display the standard deviation of the averages calculated for each simulation and trajectory.

distance of the inter-peptide chains but also affect the mechanical strength of the fibrils.^{50,51} Thus, the alteration in the H-bond number (N–H bond) directly influences its secondary structure, and the destruction of the secondary structure is expected to prevent the growth of fibrils and effectively cure AD.^{52,53} Therefore, in order to elucidate the effect of various EGCG doses on the N–H bond of $A\beta_{17-42}$, we calculated the average N–H bond of interior $A\beta_{17-42}$ (Figure 5a), $A\beta_{17-42}$ –SOL (Figure 5b), $A\beta_{17-42}$ –EGCG (Figure 5c), and EGCG–SOL (Figure 5d). For the evolution of the N–H bond for diverse components over simulation time, see Figure S7. It can be clearly seen from Figure 5a that the N–H bond of $A\beta_{17-42}$ –EGCG [N–H bond: 48 (R20), 51 (R40), 52 (R80), and 60 (R120)] decreased for all cases, compared to that of $A\beta_{17-42}$ alone in the control system (N–H bond: 69), while the corresponding loss rates of H-bonds were 30.4% (R20), 26.1% (R40), 24.6% (R80), and 11.6% (R120). Surprisingly, for the R20 system with the lowest EGCG content, the average N–H bond was the minimum, but the breaking rate of H-bonds was the maximum. The increase in the average N–H bond was demonstrated with increasing EGCG concentrations in the cases of R40, R80, and R120. The formation of H-bonds between the side peptide chains of $A\beta_{17-42}$ resulted from EGCG-mediated structural changes that compensated for the H-bond loss between the β -chains of fibrils owing to the denatured β -sheet structures. As shown in Figure 5b, compared with that of $A\beta_{17-42}$ alone in the solvent (average N–H bond: 254), the N–H bond of $A\beta_{17-42}$ –SOL with EGCG [236 (R20), 220 (R40), 239 (R80), and 203 (R120)] reduced to varying extents but did not exhibit dose-dependent trends. Despite the structural dissociation of $A\beta_{17-42}$ affected by EGCG (Figures 4a–d and 5e,f), the H-bonds with water molecules were still limited by the effective

accessible region, the solvent effect, and the direction of structural collapse of $A\beta_{17-42}$. Similarly, accompanied with the growing molar ratio of EGCG, the N–H bond of $A\beta_{17-42}$ –EGCG [19 (R20), 30 (R40), 27 (R80), and 21 (R120)] increased first and then decreased (Figure 5c), which was reflected by the limited accessible binding sites located on the surface of $A\beta_{17-42}$. It was obvious that the N–H bond [186 (R20), 373 (R40), 731 (R80), and 1038 (R120)] between EGCG and the water solvent was positively correlated with the EGCG molar ratio (Figure 5d).

Each of the five repeating monomeric peptide chains consisted of a randomly curled segment ($N_{27}KGA_{30}$) connecting two parallel and anti-parallel β -strands (B1: $L_{17}VFFAEDVGS_{26}$ and B2: $I_{31}GLMVGGVVIA_{42}$) stacked longitudinally to form $A\beta_{17-42}$. Thus, we analyzed the evolution mechanism of H-bonds and the secondary structure of $A\beta_{17-42}$ from two β -strands, B1 and B2, respectively.

As Figure 5e shows, for R20 and R40 cases, just one chain (peptide chain 1) was unzipped from the skeleton backbone. On the contrary, the self-assembled structure unlocked by two chains (both chain 1 and chain 5) led to more severe dissociation in R80 and R120 systems. Besides, the N–H bond on the side of chain 5 was more dissociated, and the structure shown was looser. EGCG-initiated structural remodeling of $A\beta_{17-42}$ primarily started from the marginal peptide chains. Figure 5f shows that after binding with the EGCG, the N–H bond and the corresponding secondary structure in the B2 fragment did not change significantly. Overall, EGCG's damage to the B1 fragment was greater than that to B2 (Figure 5e,f). Therefore, the EGCG binding altered the H-bond interaction with the limbic peptide chain, and the disappeared backbone H-bonds were mainly located in the β -sheet structure of B1. The visible distinctions in the N–H

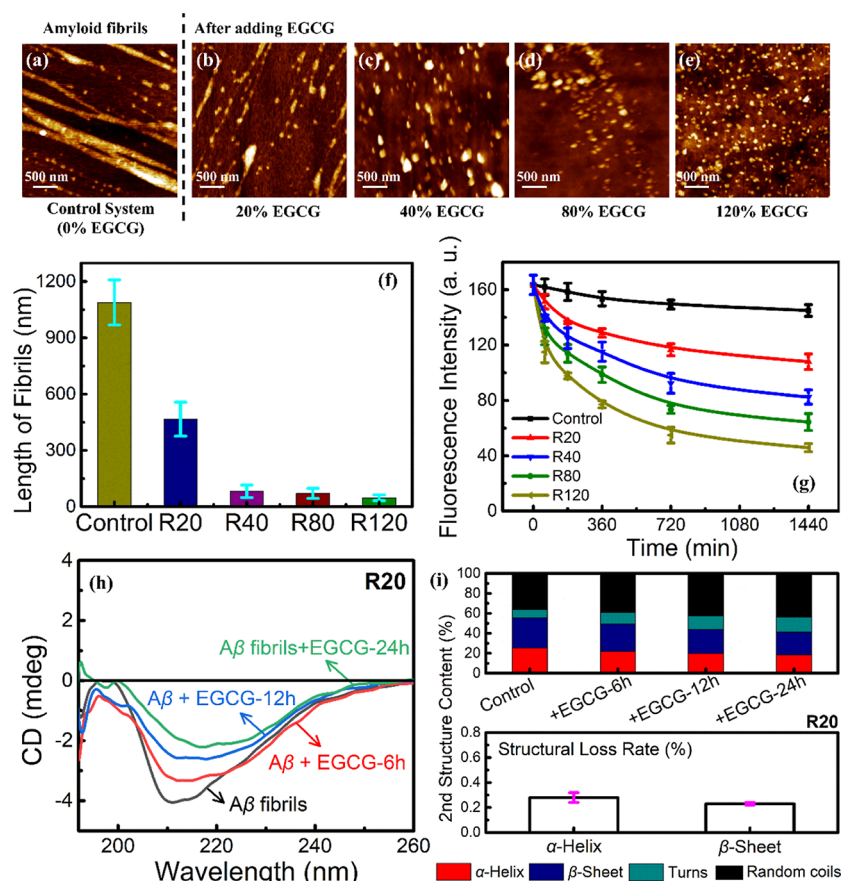


Figure 6. AFM images represent the morphology of different samples in the absence and presence of EGCG: (a) control of $A\beta_{17-42}$ aggregates. The $A\beta_{17-42}$ fibrils mixed with different concentrations of EGCG. The molar ratio of $A\beta_{17-42}$ fibrils and EGCG is 1:20 (b), 1:40 (c), 1:80 (d), and 1:120 (e). (f) Height analysis for AFM images. (g) Fibrillation kinetics of $A\beta_{17-42}$ fibrils as characterized by the ThT binding with and without EGCG. (h) Secondary structure changes of $A\beta_{17-42}$ fibrils characterized by CD spectra. The alteration in the secondary structure of $A\beta_{17-42}$ fibrils on subsequent incubation at 37 °C for 24 h. In each environment, the $A\beta_{17-42}$ fibrils formed different structures (β -sheets, helices, random coils, turns, etc.), determining the structure stability of the protein. (i) Secondary structure (denoted “2nd structure” in the images) content and the loss rate of the secondary structure in the $A\beta_{17-42}$ fibrils with addition of EGCG. Taking the R20 case as the representative and see the [Supporting Information](#) for the other cases.

bond for four systems, which tended to undermine the β -sheet structure, resulted in a sequential decrease in the β -sheet content and the extension of its structure (Figure 5e). Through the above-mentioned analysis, a profound impact on the structural stability of $A\beta$ aggregates reconstructed by EGCG in a dose-dependent manner is observed. The reduction in the β -sheet content and appearance of the backbone H-bond in the random coil structure reflected that EGCG transformed their ordered structure into a partially disordered one.

EGCG Disrupted the Preformed $A\beta_{17-42}$ Pentameric Fibrils. The above-mentioned simulation results indicated that EGCG could effectively remodel and then destabilize the structure of $A\beta_{17-42}$. To further confirm this implication macroscopically, we first utilized AFM to validate the effect of EGCG on the morphology of $A\beta_{1-42}$ fibrils (we chose $A\beta_{17-42}$ to model $A\beta_{1-42}$ for saving computing resources in the simulation) (Figure 6a–e). Figure 6a (as a control) shows that the untreated $A\beta_{1-42}$ fibrils (0.5 mg mL^{-1}) formed a typically thick and long amyloid fibrous morphology with an average fibril length (L_{fibril}) of $1088.0 \pm 120.1 \text{ nm}$ after 24 h of incubation (Figure 6f). With the addition of EGCG (corresponding to R20), most fibrils were degraded into short fibrils, and a small number of fibrils began to show some irregularity (Figure 6b). Meanwhile, average L_{fibril} was reduced

to about $466.5 \pm 90.7 \text{ nm}$ (Figure 6f). For R80, the number of fibrillar aggregates became smaller since the interaction with EGCG molecules (Figure 6d), and average L_{fibril} decreased to about $71.1 \pm 21.7 \text{ nm}$ (Figure 6f). In the presence of vast EGCG (corresponding to R120), we observed that the fibrils eventually almost completely decomposed into amorphous aggregates (Figure 6e), with an average size of about $47.5 \pm 15.3 \text{ nm}$ (Figure 6f). Overall, AFM images showed that the addition of EGCG to $A\beta$ fibrils can not only reduce the number of fibrils but also cause them to lose their fibrillar morphology and break them down into amorphous aggregates, thereby hindering the fibril growth.

Besides, ThT fluorescence experiments were conducted to measure the degradation effect of EGCG on $A\beta_{1-42}$ fibrils. Figure 6g shows the depolymerization kinetics of $A\beta_{1-42}$ fibrils after incubating for 24 h at 37 °C with different molar ratios (R20, R40, R80, and R120) of EGCG and $A\beta_{1-42}$ solutions. It can be seen from Figure 6g that the dissociation effect of EGCG on $A\beta_{1-42}$ fibers was dose-dependent. We observed that under the action of a low concentration of EGCG (corresponding to R20), the fluorescence intensity of $A\beta_{1-42}$ fibrils decreased slightly, and the final ThT signal decreased by 33% (Figure 6g). When the EGCG concentration was increased to R80, the fluorescence intensity of $A\beta_{1-42}$ fibrils

decreased significantly. At this concentration, the fluorescence intensity of the EGCG/ $A\beta_{1-42}$ mixture decreased by 55% at 12 h and decreased by 61% at 24 h (Figure 6g). When the ratio of EGCG/ $A\beta_{1-42}$ further rose to 1:120, we noted that EGCG had a stronger dissociation impact on $A\beta_{1-42}$ fibrils, and the final ThT intensity was severely reduced by 72%, which was consistent with the AFM results regarding the appearance of numerous amorphous aggregates. Moreover, previous work reported that excessively high ratios of EGCG will increase ThT intensity, which was attributed to the assembly of EGCG itself which will reduce its inhibitory capability.^{54–56}

The secondary structure of amyloid fibrils is also an important quantity for characterizing $A\beta_{1-42}$ fibrillation and decomposition. CD was used to measure alterations in the secondary structure of EGCG-treated $A\beta_{1-42}$ fibrils (Figure 6h). The characteristic β -sheet structure (negative peak at 210 nm) of $A\beta_{1-42}$ fibrils was clearly observed by the CD spectrum. The CD signal intensity of the $A\beta_{1-42}$ fibril alone at its maximum absorption peak ($\lambda_{\max} = 210$ nm) was 4.1 ± 0.2 mdeg. Taking R20 as an example, the intensity of the $A\beta_{1-42}$ fibril decreased with enhancing EGCG-treated time [from 3.4 ± 0.2 (6 h, $\lambda_{\max} = 212$ nm) to 2.6 ± 0.1 (12 h, $\lambda_{\max} = 214$ nm) and 2.3 ± 0.1 (24 h, $\lambda_{\max} = 216$ nm)], and the maximum absorption peak developed a red shift (Figure 6h). This may be caused by the benzene ring with electron-rich properties introduced in EGCG, forcing π - π interaction between EGCG and the aromatic AA in the $A\beta_{1-42}$ fibril. Figure 6i reveals the changes in the different types of secondary structure contents. We noticed that the contents of the α -helix and β -sheet decreased sequentially over time, and the compositions of turns and random coil structures increased in sequence. At this concentration, the structural loss rates of the α -helix and β -sheet induced by EGCG were 27.3 and 23.0%, respectively. Moreover, with the increase in the molar ratio, the structural loss rate of $A\beta_{1-42}$ fibrils also increased (Figure S11). These outcomes demonstrated that the gradual dissolution of the β -sheet structure during the decomposition process converts into a random coil structure, which was consistent with the previous MD results. In short, the above-mentioned experimental results confirmed that EGCG was indeed an effective $A\beta_{1-42}$ fibril inhibitor. EGCG can induce conformational rearrangement of $A\beta_{1-42}$ fibrils and has a strong dissolution effect and then triggers the disintegration of fibrils in a dose-dependent manner.

Primarily Specific Binding of EGCG toward the Ordered Structure of $A\beta_{17-42}$ and Conformed to the Structural Change. To determine the predominant binding site and fully figure out the remodeling mechanism of the $A\beta_{17-42}$ oligomer mediated by EGCG, we analyzed the binding energy of EGCG to each AA residue on $A\beta_{17-42}$. As observed from Figure 7, the binding energy of EGCG molecules to L17, F20, I31, M35, V36, and other hydrophobic residues was stronger than that of the other types of AAs, indicating that the hydrophobic interaction and aromatic stacking played an important role in the formation and stabilization of $A\beta_{17-42}$ fibrils, which showed good agreement with the experimental observation.^{57,58} The binding energy contribution of EGCG to D23 was also strong, which was most likely caused by the formation of a H-bond with EGCG. The three most favorable binding domains of $A\beta_{17-42}$ were L₁₇VFFA₂₁ (interaction site 1, denoted S1), I₃₁I₃₁GLMV₃₆ (interaction site 2, denoted S2), and V₃₉VIA₄₂ (interaction site 3, denoted S3). For the R80 system (as a representative), by analyzing the binding energy

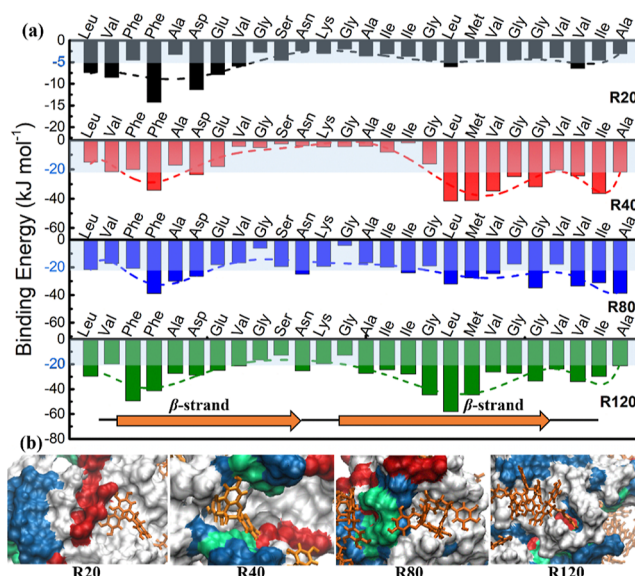


Figure 7. (a) Detailed binding energy of EGCG and $A\beta_{17-42}$ in four cases. (b) Representative snapshots of the interaction modes between EGCG and $A\beta_{17-42}$ are presented. The color of EGCG is encoded in dark yellow.

of these three sites, we found that the average binding energy of the S3 site was the highest (-120.98 ± 6.48 kJ mol⁻¹), while S1 (-128.51 ± 4.48 kJ mol⁻¹) and S2 (-146.78 ± 9.76 kJ mol⁻¹) had stronger binding energy, demonstrating that these two regions were the most favorable sites for EGCG binding. Taking the S1 site as an example, for the R20 system, the average binding energy was -30.91 ± 3.25 kJ mol⁻¹, and in the R120 system, the average binding energy reduced to -167.57 ± 9.57 kJ mol⁻¹. Therefore, more EGCG molecules will bind to the hydrophobic or hydrophilic sites on the surface of amphiphilic $A\beta_{17-42}$ and contribute to its structural transformation.

A representative snapshot of the $A\beta_{17-42}$ -EGCG interaction mode is shown in Figure 7. EGCG was in favor of interacting with domains rich in the β -sheet structure. For example, the binding energy of β -strand fragments is significantly stronger than that of N₂₇KGA₃₀. S1 was on the B1 side, and S2 and S3 are on the anti-parallel B2 side. First, we analyzed the interaction characteristics of EGCG and the S1 site. Obviously, partial EGCG was embedded and stayed in a hydrophobic pocket constituted by VAL18, Phe 20, and ALA21 distributed on different peptide chains. The formation of this pocket perturbed the well-organized surface of $A\beta_{17-42}$ and interfered with its β -sheet content to further reduce structural stability. At the S2 site, the trihydroxyphenyl group of EGCG tended to be attracted between peptide chains at the sites with strong hydrophobic interactions such as Leu34, Val36, and ILE41. Because S2 and S3 were adjacent and S3 was located at the end of the peptide chain, EGCG bound to the “turn” structure at the end of $A\beta_{17-42}$ and embedded in the S3 site. Since all three sites were located in the growth direction of fibril seeds, binding to EGCG may effectively block the growth of $A\beta_{17-42}$ pentameric fibrils. From the above-mentioned analysis, it can be seen that among the three sites identified initially, S2 and S3 tended to be most favorable binding sites. Driven by hydrophobic interaction, vdW interaction, and H-bonding, EGCG strongly bound to $A\beta_{17-42}$, which restructured the fibrils by destroying the interchain H-bonds and secondary

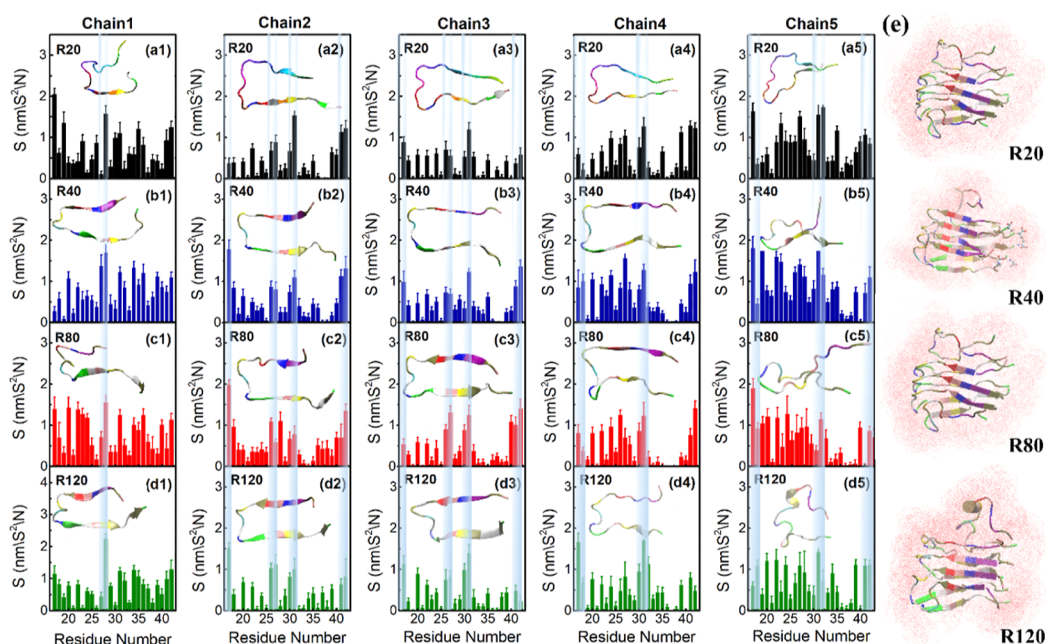


Figure 8. EGCG-dependent alteration in solvent accessible areas at the surface of the AAs of each peptide chain in $A\beta_{17-42}$ in the four cases [(a), R20; (b), R40; (c), R80; and (d), R120]. The light blue illustrates the solvent accessible surface area of AA residues in each peptide chain of $A\beta_{17-42}$ with EGCG. (e) Representative snapshot of solvent distribution in the 1 nm range around the surface of $A\beta_{17-42}$ pentameric fibrils. Water molecules are shown in red.

structure of the fibril (Figures 4 and 5), which agreed with the experimental results.^{59,60} In general, the structural characteristics of the drug, for example, the geometry and H-bond binding sites, will cause the small molecule to partially or completely wedge into the grooves formed by peptide chains, which will weaken the non-bonded interaction within $A\beta_{17-42}$ and disrupt the ordered β -chain (Figure 7). Furthermore, previous studies have also shown that there were significant differences in saturation between the four rings of EGCG, and rings A and B were the main contact sites with the $A\beta_{17-42}$ oligomer.^{61,62}

Reduced Solvent Accessible Surface of $A\beta_{17-42}$ Pentameric Fibrils upon Binding. To investigate the effect of EGCG molecules on the interpeptide interaction [including the lateral chain (LC) and inside chain (IC)], we calculated the sum of solvent accessible surface area (S_{tot}) on the surface of each peptide chain in the $A\beta_{17-42}$ pentameric fibrils. As shown in Figures 8a and S9, S_{tot} of $A\beta_{17-42}$ with EGCG significantly reduced compared to that of $A\beta_{17-42}$ alone, which meant that the interaction between $A\beta_{17-42}$ and EGCG led to rapid desolvation of the peptide aggregates. However, we noted that S_{tot} of lateral monomeric peptide chains (chain 1 and chain 5) in the control system was 18.12 ± 0.22 and 17.34 ± 0.19 nm² (Figure S9a,e). After EGCG associated with the $A\beta_{17-42}$ surface, average S_{tot} of chain 1 increased to 18.49 ± 0.15 nm² (R20), 19.21 ± 0.13 nm² (R40), 19.81 ± 0.14 nm² (R80), and 20.74 ± 0.18 nm² (R120) (Figure 8a1–d1). Similarly, for chain 5, its average S_{tot} value increased continuously from 17.72 ± 0.18 nm² (R20) to 23.27 ± 0.14 nm² (R120) (Figure 8a5–d5), which indicated that the marginal peptide chain can induce a larger hydration shell (Figure 8e). In contrast, S_{tot} in the remaining peptide chains decreased upon the binding of EGCG. Taking chain 3 as an example, $A\beta_{17-42}$ decreased from 12.28 ± 0.11 nm² (control) to 11.78 ± 0.10 nm² (R20), 11.63 ± 0.15 nm² (R40), 10.64 ± 0.10 nm² (R80), and 9.21 ± 0.09 nm² (R120) (Figures 8a3–

d3 and S9c). Overall, EGCG induced a decrease in S_{tot} of $A\beta_{17-42}$. The increase in S_{tot} of the LC was attributed to the combinational effect of the EGCG binding and the solvent-mediated interaction, while the decrease in S_{tot} of IC was primarily due to the inducement of EGCG. Therefore, the EGCG molecules mainly interfered with the interaction on the IC in $A\beta_{17-42}$ and broke the H-bonds between the peptide chains.

After proving the crucial role of EGCG in the interaction of $A\beta_{17-42}$ peptide chains, we further analyzed the solvent accessible surface area (S_{AA}) of each AA residue in the peptide chains to evaluate interactive affinity between different AAs and EGCG. Despite the limited hydrophobic/hydrophilic sites at the surface of $A\beta_{17-42}$ and the steric effect, the further increase in EGCG can enhance S_{AA} after EGCG adsorbed on the $A\beta$'s surface. It is observed in Figures 8 and S9 that with EGCG molecules, S_{AA} of the hydrophilic region ($A_{22}\text{EDVGS}_{27}$) greatly increased from 16.43 ± 0.75 nm² (control) to 18.92 ± 0.65 nm² (R20), 20.86 ± 0.87 nm² (R40), 21.44 ± 0.14 nm² (R80), and 22.69 ± 0.61 nm² (R120). In contrast, the C-terminal hydrophobic region [$(G_{33}\text{LMVGGVVI}_{41})$] (S_{AA} (19.83 ± 0.80 nm² (control), 19.64 ± 0.49 nm² (R20), 19.88 ± 0.46 nm² (R40), 16.37 ± 0.57 nm² (R80), and 18.36 ± 0.50 nm² (R120)) and CHC region [16.84 ± 0.69 nm² (control), 16.51 ± 0.73 nm² (R20), 14.93 ± 0.56 nm² (R40), 13.66 ± 0.83 nm² (R80), and 12.46 ± 0.54 nm² (R120)] remained relatively low. S_{AA} of C-terminal AA sequences and the CHC region was smaller than that of the hydrophilic domains, demonstrating that EGCG was principally bound with $A\beta_{17-42}$. The presence of EGCG would exclude the water molecules surrounding the fibrils, hindering the peptide–water interaction and thus enhancing the binding capability of peptide chains and EGCG. The β -sheet structure of $A\beta_{17-42}$ decreased with the increase in the EGCG concentration. Moreover, although the C-terminal hydrophobic region had a larger volume, it was clear that EGCG

had a stronger spatial shielding effect on the central hydrophobic region than that at the C-terminal. These different phenomena were attributed to the interfacial properties of $A\beta_{17-42}$ and the polarity of AA residues. We also found that during the interaction of the EGCG benzene ring with $A\beta_{17-42}$, the solvation loss around the small molecules of EGCG was even more pronounced and that EGCG was buried in the pockets and gaps of the fibrils.

Furthermore, for $A\beta_{17-42}$, the β -sheet was mostly located in the CHC domains and the C-terminal hydrophobic region (including $G_{33}LMV_{36}$ and $G_{38}VVI_{41}$ domains), and these two regions played a critical role in the assembly of the monomeric peptide chain. It can be seen that in the presence of EGCG, the contact between the CHC regions and C-terminal hydrophobic region in the edge peptide chain of $A\beta_{17-42}$ almost disappeared. Combined with the above-mentioned results, we can conclude that EGCG molecules had strong interaction with these two regions of $A\beta_{17-42}$, and $A\beta$ fibrillation can be effectively impeded by EGCG binding.

CONCLUSIONS

In summary, we reported that EGCG with hydrophobic (aromatic ring) and hydrophilic (phenolic hydroxyl) moieties could mediate structural rearrangement of $A\beta$ fibrils and evoked a strong decomposition effect by performing intensive all-atom MD simulations. EGCG's strong dispersion of $A\beta$ fibers was collaboratively driven by electrostatic and vdW interaction. Moreover, EGCG reshaped the $A\beta$ molecular configuration by disrupting the β -sheet structure and the H-bonds between internal peptide chains, especially the parallel β -strand ($L_{17}VFFAEDVGS_{26}$). The mechanism revealed through computational modeling was also validated by experimental observations. The results of AFM images, ThT fluorescence, and CD spectra verified that EGCG would significantly reduce the amount of $A\beta$ fibrils and transform them into amorphous aggregates. We also showed that EGCG-mediated $A\beta_{17-42}$ binding was a multisite binding driver, of which the hydrophobic $I_{31}IGLMV_{36}$ and C-terminal $V_{39}VIA_{42}$ regions were the two most favorable binding sites. The sequence-specific binding energy of EGCG molecules with AA residues showed that hydrophobic residues played a vital role in the EGCG binding process. Finally, the desolvation of $A\beta_{17-42}$ upon binding appears to cause direct contact between EGCG and the $A\beta$ surface, causing H-bond interaction within $A\beta_{17-42}$ to be disturbed. Although the current work is focused on $A\beta$ fibrils, a similar mechanism applies to other types of β -sheet-rich fibrillar aggregates. Especially, we expect that EGCG as a green inhibitor-based dissociation mechanism based on "structural remodeling" can stimulate and promote novel and rational drug design and development.

ASSOCIATED CONTENT

Supporting Information

The Supporting Information is available free of charge at <https://pubs.acs.org/doi/10.1021/acsomega.2c05995>.

Geometry optimization and structural parameterization for the small-molecule drug candidate, system model design and MD simulation methods for $A\beta_{17-42}$ fibril-EGCG interactions, culture and the disaggregation process of the amyloid fibril affected by EGCG tracked by CD, AFM, and ThT detection, structural redirection (rmsd, R_g , no. of contact, RMSF, etc.) and detailed

conformational evolution of $A\beta_{17-42}$ alone and $A\beta_{17-42}$ pentameric fibrils with EGCG, solvent accessible surface of $A\beta_{17-42}$ pentameric fibrils without EGCG, experimental results of AFM and CD confirming the formation of $A\beta$ aggregates, and EGCG disrupting the secondary structure of preformed $A\beta_{1-42}$ pentameric fibrils (PDF)

AUTHOR INFORMATION

Corresponding Authors

Nan Zhang – School of Chemistry and Chemical Engineering, Xi'an University of Science and Technology, Xi'an 710054, China; orcid.org/0000-0002-5412-8398; Email: zhangn1123@126.com

Yuan Cheng – Monash Suzhou Research Institute, Monash University, Suzhou 215000, China; Department of Materials Science and Engineering, Monash University, Melbourne 3800 Victoria, Australia; orcid.org/0000-0003-0061-3934; Email: yuan.cheng@monash.edu

Authors

Chaoren Yan – School of Medicine, Key Laboratory for Molecular Genetic Mechanisms and Intervention Research on High Altitude Disease of Tibet Autonomous Region, Xizang Minzu University, Xianyang 712082, China; orcid.org/0000-0002-5055-1893

Changji Yin – Monash Suzhou Research Institute, Monash University, Suzhou 215000, China; Department of Materials Science and Engineering, Monash University, Melbourne 3800 Victoria, Australia

Xiaoling Hu – School of Chemistry and Chemical Engineering, Northwestern Polytechnical University, Xi'an 710072, China

Ping Guan – School of Chemistry and Chemical Engineering, Northwestern Polytechnical University, Xi'an 710072, China

Complete contact information is available at:

<https://pubs.acs.org/10.1021/acsomega.2c05995>

Notes

The authors declare no competing financial interest.

ACKNOWLEDGMENTS

N.Z. from Xi'an University of Science and Technology is grateful for start-up research funds. X.H. from Northwestern Polytechnical University is grateful for the financial support from the China Scholarship Council, National Natural Science Foundation of China (grant no. 51433008).

REFERENCES

- (1) Power, R.; Prado-Cabrero, A.; Mulcahy, R.; Howard, A.; Nolan, J. M. The Role of Nutrition for the Aging Population: Implications for Cognition and Alzheimer's Disease. *Annu. Rev. Food Sci. Technol.* **2019**, *10*, 619–639.
- (2) Gaugler, J.; James, B.; Johnson, T.; Marin, A.; Weuve, J. 2021 Alzheimer's Disease Facts and Figures. *Alzheimer's Dementia* **2021**, *17*, 327–406.
- (3) Barthélemy, N.; Li, Y.; Li, N.; Joseph-Mathurin, B. A.; Gordon, J.; et al. A Soluble Phosphorylated Tau Signature Links Tau, Amyloid and the Evolution of Stages of Dominantly Inherited Alzheimer's Disease. *Nat. Med.* **2020**, *26*, 398–407.
- (4) Santiago, J. A.; Potashkin, J. A. The Impact of Disease Comorbidities in Alzheimer's Disease. *Front. Aging Neurosci.* **2021**, *13*, 631770.
- (5) Poovaiyah, N.; Davoudi, Z.; Peng, H.; Schlichtmann, S.; Mallapragada, M.; Narasimhan, N.; Wang, Q. Treatment of

- Neurodegenerative Disorders through the Blood-Brain Barrier using Nanocarriers. *Nanoscale* **2018**, *10*, 16962–16983.
- (6) Hochdörffer, K.; März-Berberich, J.; Nagel-Steger, L.; Eppler, M.; Meyer-Zaika, W.; Horn, A. H. C.; et al. Rational Design of β -sheet Ligands against $A\beta_{42}$ -induced Toxicity. *J. Am. Chem. Soc.* **2011**, *133*, 4348–4358.
- (7) Wang, X.; Sun, G.; Feng, T.; Zhang, J.; Huang, X.; et al. Sodium oligomannate therapeutically remodels gut microbiota and suppresses gut bacterial amino acids-shaped neuroinflammation to inhibit Alzheimer's disease progression. *Cell Res.* **2019**, *29*, 787–803.
- (8) Makin, S. The Amyloid Hypothesis on Trial. *Nature* **2018**, *559*, S4–S7.
- (9) Lu, P.; Bai, X. C.; Ma, D.; Xie, T.; Yan, C.; Sun, L.; Yang, G.; Zhao, Y.; Zhou, R.; Scheres, S. H. W.; Shi, Y. Three-dimensional structure of human γ -secretase. *Nature* **2014**, *512*, 166.
- (10) Panza, F.; Lozupone, M.; Bellomo, A.; Imbimbo, B. P. Do anti-amyloid- β drugs affect neuropsychiatric status in Alzheimer's disease patients? *Ageing Res. Rev.* **2019**, *55*, 100948.
- (11) Yang, C.; Xiao, S. New developments of clinical trial in immunotherapy for Alzheimer's disease. *Curr. Pharm. Biotechnol.* **2015**, *16*, 484–491.
- (12) Ling, S.; Chen, W.; Fan, Y.; Zheng, K.; Jin, D. L.; Yu, H.; Buehler, M. J.; Kaplan, D. L. Biopolymer nanofibrils: Structure, modeling, preparation, and applications. *Prog. Polym. Sci.* **2018**, *85*, 1–56.
- (13) Howard, R.; Liu, K. Y. Questions emerge as Biogen claims aducanumab turnaround. *Nat. Rev. Neurol.* **2020**, *16*, 63.
- (14) Wang, W.; Zhao, G.; Dong, X.; Sun, Y. Unexpected Function of a Heptapeptide-Conjugated Zwitterionic Polymer that Coassembles into β -Amyloid Fibrils and Eliminates the Amyloid Cytotoxicity. *ACS Appl. Mater. Interfaces* **2021**, *13*, 18089–18099.
- (15) Shuaib, S.; Narang, S. S.; Goyal, D.; Goyal, B. Computational design and evaluation of β -sheet breaker peptides for destabilizing Alzheimer's amyloid- β 42 protofibrils. *J. Cell. Biochem.* **2019**, *120*, 17935.
- (16) Adessi, C.; Soto, C. Beta-sheet breaker strategy for the treatment of Alzheimer's disease. *Drug Develop. Res.* **2002**, *56*, 184–193.
- (17) Wang, H.; Sui, H.; Zheng, Y.; Jiang, Y.; Shi, Y.; Liang, J.; Zhao, L. Curcumin-primed exosomes potentially ameliorate cognitive function in AD mice by inhibiting hyperphosphorylation of the Tau protein through the AKT/GSK-3 β pathway. *Nanoscale* **2019**, *11*, 7481–7496.
- (18) Kechko, O.; Petrushanko, I.; Piatkov, K.; Mitkevich, V.; Makarov, A. Apoptosis-inducing effect of $A\beta$ peptides is associated with inhibition of N-end rule pathway. *Alzheimer's Dementia* **2018**, *14*, P357.
- (19) Shaham-Niv, S.; Rehak, P.; Zaguri, D.; Levin, A.; Adler-Abramovich, L.; Vuković, L.; Král, P.; Gazit, E. Differential inhibition of metabolite amyloid formation by generic fibrillation-modifying polyphenols. *Chem. Commun.* **2018**, *1*, 25.
- (20) Ren, B.; Zhang, Y.; Zhang, M.; Liu, Y.; Zhang, D.; Gong, X.; Feng, Z.; Tang, J.; Chang, Y.; Zheng, J. Fundamentals of cross-seeding of amyloid proteins: an introduction. *J. Mater. Chem. B* **2019**, *7*, 7267–7282.
- (21) Kallinen, A.; Adamcik, J.; Wang, W.; Ge, X.; Mezzenga, R.; Davis, T. P.; et al. Nanoscale inhibition of polymorphic and ambidextrous IAPP amyloid aggregation with small molecules. *Nano Res.* **2018**, *11*, 3636–3647.
- (22) Brahmachari, S.; Arnon, Z. A.; Frydman-Marom, A.; Gazit, E.; Adler-Abramovich, L. Diphenylalanine as a Reductionist Model for the Mechanistic Characterization of β -Amyloid Modulators. *ACS Nano* **2017**, *11*, S960–S969.
- (23) Young, L. M.; Saunders, J. C.; Mahood, R. A.; Revill, C. H.; Foster, R. J.; Tu, L. H.; et al. Screening and classifying small-molecule inhibitors of amyloid formation using ion mobility spectrometry-mass spectrometry. *Nat. Chem.* **2015**, *7*, 73.
- (24) Ling, S.; Li, C.; Adamcik, J.; Shao, Z.; Chen, X.; Mezzenga, R. Modulating Materials by Orthogonally Oriented β -Strands: Composites of Amyloid and Silk Fibroin Fibrils. *Adv. Mater.* **2014**, *26*, 4569–4574.
- (25) Kian, K.; Khalatbary, A. R.; Ahmadvand, H.; Karimpour Malekshah, A.; Shams, Z. Neuroprotective effects of (–)-epigallocatechin-3-gallate (EGCG) against peripheral nerve transection-induced apoptosis. *Nutr. Neurosci.* **2019**, *22*, 578–586.
- (26) Debnath, K.; Shekhar, S.; Kumar, V.; Jana, N. R.; Jana, N. R. Efficient inhibition of protein aggregation, disintegration of aggregates, and lowering of cytotoxicity by green tea polyphenol-based self-assembled polymer nanoparticles. *ACS Appl. Mater. Interfaces* **2016**, *8*, 20309–20318.
- (27) Alred, E. J.; Phillips, M.; Berhanu, W. M.; Hansmann, U. On the lack of polymorphism in $A\beta$ -peptide aggregates derived from patient brains. *Protein Sci.* **2015**, *24*, 923–935.
- (28) Xi, W.; Hansmann, U. H. E. Conversion between parallel and antiparallel β -sheets in wild-type and Iowa mutant $A\beta_{40}$ fibrils. *J. Chem. Phys.* **2018**, *148*, 045103.
- (29) Nasica-Labouze, J.; Nguyen, P. H.; Sterpone, F.; Berthoumieu, O.; Buchete, N.; et al. Amyloid β Protein and Alzheimer's Disease: When Computer Simulations Complement Experimental Studies. *Chem. Rev.* **2015**, *115*, 3518–3563.
- (30) Ahmed, R.; VanSchouwen, B.; Jafari, N.; Ni, X.; Ortega, J.; Melacini, G. Molecular Mechanism for the (–)-Epigallocatechin Gallate-Induced Toxic to Nontoxic Remodeling of $A\beta$ Oligomers. *J. Am. Chem. Soc.* **2017**, *139*, 13720–13734.
- (31) Xiao, Y.; Matsuda, I.; Inoue, M.; Sasahara, T.; Hoshi, M.; Ishii, Y. NMR-based site-resolved profiling of β -amyloid misfolding reveals structural transitions from pathologically relevant spherical oligomer to fibril. *J. Biol. Chem.* **2020**, *295*, 458–467.
- (32) Fontana, F.; Gelain, F. Probing mechanical properties and failure mechanisms of fibrils of self-assembling peptides. *Nanoscale Adv.* **2020**, *2*, 190–198.
- (33) Yin, X.; Yang, J.; Xiao, F.; Yang, Y.; Shen, H. B. MemBrain: An Easy-to-Use Online Webserver for Transmembrane Protein Structure Prediction. *Nano-Micro Lett.* **2018**, *10*, 2.
- (34) Hong, C.; Liang, J.; Xia, J.; Zhu, Y.; Guo, Y.; Wang, A.; Lu, C.; Ren, H.; Chen, C.; Li, S.; Wang, D.; Zhan, H.; Wang, J. One Stone Four Birds: A Novel Liposomal Delivery System Multi-functionalized with Ginsenoside Rh2 for Tumor Targeting Therapy. *Nano-Micro Lett.* **2020**, *12*, 129.
- (35) Liu, H.; Liu, X.; Zhou, S.; An, X.; Liu, H.; Yao, X. Disclosing the Template-Induced Misfolding Mechanism of Tau Protein by Studying the Dissociation of the Boundary Chain from the Formed Tau Fibril Based on a Steered Molecular Dynamics Simulation. *ACS Chem. Neurosci.* **2019**, *10*, 1854–1865.
- (36) Ahmed, R.; VanSchouwen, B.; Jafari, N.; Ni, X.; Ortega, J.; Melacini, G. Molecular Mechanism for the (–)-Epigallocatechin Gallate-Induced Toxic to Nontoxic Remodeling of $A\beta$ Oligomers. *J. Am. Chem. Soc.* **2017**, *139*, 13720–13734.
- (37) Matthes, D.; Gapsys, V.; Griesinger, C.; de Groot, B. D. Resolving the atomistic modes of Anle138b inhibitory action on peptide oligomer formation. *ACS Chem. Neurosci.* **2017**, *8*, 2791–2808.
- (38) Dennington, R.; Keith, T.; Millam, J. *GaussView*, version 5; Semicem Inc.: Shawnee Mission, KS, 2009.
- (39) Jensen, F. *Introduction to Computational Chemistry*; John Wiley & Sons, 2017.
- (40) Frisch, M. J.; Trucks, G. W.; Schlegel, H. B.; Scuseria, G. E.; Robb, M. A.; et al. *Gaussian 16*, Revision A. 03; Gaussian, Inc.: Wallingford CT, 2016.
- (41) Wang, J.; Cieplak, P.; Kollman, P. A. How well does a restrained electrostatic potential (RESP) model perform in calculating conformational energies of organic and biological molecules? *J. Comput. Chem.* **2000**, *21*, 1049–1074.
- (42) Du, J.; Qiu, M.; Guo, L.; Yao, X. Computational study of the binding mechanism between farnesoid X receptor α and antagonist N-benzyl-N-(3-(tertbutyl)-4-hydroxyphenyl)-2,6-dichloro-4-(dimethylamino) benzamide. *J. Biomol. Struct. Dyn.* **2019**, *37*, 1628–1640.

- (43) Lühns, T.; Ritter, C.; Adrian, M.; Riek-Loher, D.; Bohrmann, B.; Döbeli, H.; Schubert, D.; Riek, R. 3D structure of Alzheimer's amyloid-beta(1-42) fibrils. *Proc. Natl. Acad. Sci. U.S.A.* **2005**, *102*, 17342.
- (44) Hess, B.; Kutzner, C.; van der Spoel, D.; Lindahl, E. GROMACS 4: Algorithms for Highly Efficient, Load-balanced, and Scalable Molecular Simulation. *J. Chem. Theory Comput.* **2008**, *4*, 435–447.
- (45) Duan, Y.; Wu, C.; Chowdhury, S.; Lee, M. C.; Xiong, G.; Zhang, W.; Yang, R.; Cieplak, P.; Luo, R.; Lee, T.; Caldwell, J.; Wang, J.; Kollman, P. A Point-charge Force Field for Molecular Mechanics Simulations of Proteins Based on Condensed-phase Quantum Mechanical Calculations. *J. Comput. Chem.* **2003**, *24*, 1999–2012.
- (46) Price, D. J.; Brooks, C. L. A modified TIP3P water potential for simulation with Ewald summation. *J. Chem. Phys.* **2004**, *121*, 10096–10103.
- (47) Bussi, G.; Donadio, D.; Parrinello, M. Canonical sampling through velocity rescaling. *J. Chem. Phys.* **2007**, *126*, 014101.
- (48) Berendsen, H. J.; Postma, J. V.; van Gunsteren, W. F.; DiNola, A. J. R.; Haak, J. R. Molecular dynamics with coupling to an external bath. *J. Chem. Phys.* **1984**, *81*, 3684–3690.
- (49) Hess, B.; Bekker, H.; Berendsen, H. J.; Fraaije, J. G. E. M. LINCS: a linear constraint solver for molecular simulations. *J. Comput. Chem.* **1997**, *18*, 1463–1472.
- (50) Darden, T.; York, D.; Pedersen, L. Particle mesh Ewald: An $N \log(N)$ method for Ewald sums in large systems. *J. Chem. Phys.* **1993**, *98*, 10089–10092.
- (51) Humphrey, W.; Dalke, A.; Schulten, K. VMD: visual molecular dynamics. *J. Mol. Graph.* **1996**, *14*, 33–38.
- (52) Frishman, D.; Argos, P. Knowledge-based Protein Secondary Structure Assignment. *Proteins: Struct., Funct., Genet.* **1995**, *23*, 566–579.
- (53) Hooft, R. W.; Sander, C.; Scharf, M.; et al. The PDBFINDER Database: A Summary of PDB, DSSP and HSSP Information with Added Value. *Bioinform* **1996**, *12*, 525–529.
- (54) Wang, S. T.; Lin, Y.; Spencer, R. K.; Thomas, R.; Nguyen, A.; et al. Sequence-Dependent Self-Assembly and Structural Diversity of Islet Amyloid Polypeptide-Derived β -Sheet Fibrils. *ACS Nano* **2017**, *11*, 8579–8589.
- (55) Luo, L.; Gui, X.; Zhou, H.; Gu, L.; Li, Y.; Liu, X.; Zhao, M.; Li, D.; Li, X.; Liu, C. Atomic structures of FUS LC domain segments reveal bases for reversible amyloid fibril formation. *Nat. Struct. Mol. Biol.* **2018**, *25*, 341–346.
- (56) Escobedo, A.; Topal, B.; Kunze, M.; Aranda, J.; Chiesa, X.; Mungianu, D.; Bernardo-Seisdedos, G.; Eftekharzadeh, B.; Gairi, M.; Pierattelli, R.; Felli, I. C.; Diercks, T.; Millet, O.; García, J.; Orozco, M.; Crehuet, R.; Lindorff-Larsen, K.; Salvatella, X. Side chain to main chain hydrogen bonds stabilize a polyglutamine helix in a transcription factor. *Nat. Commun.* **2019**, *10*, 2034.
- (57) Ehrnhoefer, D. E.; Bieschke, J.; Boeddrich, A.; et al. EGCG redirects amyloidogenic polypeptides into unstructured, off-pathway oligomers. *Nat. Struct. Mol. Biol.* **2008**, *15*, 558.
- (58) Yan, C.; Zhang, N.; Guan, P.; Chen, X.; Ding, C.; Hou, T.; Hu, X.; Wang, J.; Wang, C. Drug-based magnetic imprinted nanoparticles: Enhanced lysozyme amyloid fibrils cleansing and anti-amyloid fibrils toxicity. *Int. J. Biol. Macromol.* **2020**, *153*, 723–735.
- (59) Nirmalraj, P. N.; List, J.; Battacharya, S.; Howe, G.; Xu, M.; Thompson, D.; Mayer, M. Complete aggregation pathway of amyloid β (1-40) and (1-42) resolved on an atomically clean interface. *Sci. Adv.* **2020**, *6*, No. eaaz6014.
- (60) Gabryelczyk, B.; Cai, H.; Shi, X.; Sun, Y.; Swinkels, P.; Salentinig, S.; Pervushin, K.; Miserez, A. Hydrogen bond guidance and aromatic stacking drive liquid-liquid phase separation of intrinsically disordered histidine-rich peptides. *Nat. Commun.* **2019**, *10*, 5465.
- (61) Liberta, F.; Loerch, S.; Rennegarbe, M.; Schierhorn, A.; Westermark, M.; Westermark, G. T.; Hazenberg, B. P. C.; Grigorieff, N.; Fändrich, M.; Schmidt, M. Cryo-EM fibril structures from systemic AA amyloidosis reveal the species complementarity of pathological amyloids. *Nat. Commun.* **2019**, *10*, 1104.
- (62) Pradeepkiran, J. A.; Reddy, P. H. Structure based design and molecular docking studies for phosphorylated tau inhibitors in Alzheimer's disease. *Cells* **2019**, *8*, 260.